

Surface-polarization-induced formation of amorphous foliaceous SiO₂ helical nanobelts

L. Z. Liu, X. L. Wu, Z. Y. Zhang, T. H. Li, and Paul K. Chu

Citation: *Appl. Phys. Lett.* **94**, 253110 (2009); doi: 10.1063/1.3160736

View online: <http://dx.doi.org/10.1063/1.3160736>

View Table of Contents: <http://apl.aip.org/resource/1/APPLAB/v94/i25>

Published by the [American Institute of Physics](http://www.aip.org).

Additional information on *Appl. Phys. Lett.*

Journal Homepage: <http://apl.aip.org/>

Journal Information: http://apl.aip.org/about/about_the_journal

Top downloads: http://apl.aip.org/features/most_downloaded

Information for Authors: <http://apl.aip.org/authors>

ADVERTISEMENT

a sampling of our products		for surface and materials science	www. rbdinstruments .com	celebrating over 20 years of innovation
 deposition tools	 desorption systems	 sputter ion sources	 viewports	 usb picoammeters

Surface-polarization-induced formation of amorphous foliaceous SiO₂ helical nanobelts

L. Z. Liu,¹ X. L. Wu,^{1,a)} Z. Y. Zhang,¹ T. H. Li,¹ and Paul K. Chu^{2,a)}

¹Department of Physics and Nanjing National Laboratory of Microstructures, Nanjing University, Nanjing 210093, People's Republic of China

²Department of Physics and Materials Science, City University of Hong Kong, Tat Chee Avenue, Kowloon, Hong Kong

(Received 23 May 2009; accepted 9 June 2009; published online 24 June 2009)

Amorphous foliaceous SiO₂ helical nanobelts with equidistant alternating bright and dark stripes are synthesized using thermal evaporation. A very thin polar crystalline layer spontaneously formed on the nanobelt surface stabilizes the twist and the internal shear stress imbalance induces the periodic reconstruction. The periodic bright and dark stripes disappear slowly with growth time because the polar crystalline SiO₂ layers are covered slowly by an amorphous layer. The polar surface-driven mechanism, which can adequately explain the appearance and disappearance of the periodic fringes, is verified theoretically. © 2009 American Institute of Physics. [DOI: 10.1063/1.3160736]

The growth and properties of nanostructures have attracted much attention in recent years because of their interesting optical and electrical properties, as well as potential applications to nanoelectronics, nanomechanics, and optoelectronics.^{1–5} As a quasi-one-dimensional nanostructure, the helical nanobelts exhibit a unique growth direction and typical rectangular cross section.^{6–9} Helical Si oxide and Si nanostructures are important microelectronics materials,^{10,11} and some helical Si oxide nanostructures have been obtained to investigate the formation process and physical properties.^{12–14} In this letter, we report the fabrication of helical amorphous SiO₂ nanobelts using a thermal evaporation technique. Different from other nanobelts,^{15,16} the periodic bright and dark stripes on the amorphous twisted SiO₂ nanobelts surface disappear if the fabrication time is long. To better understand the phenomenon and the formation mechanism of the helical amorphous SiO₂ nanobelts stripes, the formation process is simulated. The formation mechanism can explain some experimental phenomena about stripes formation pertaining to amorphous nanobelts, which are obviously different from the stripes on ZnO nanobelts observed by transmission electron microscopy.^{17–19}

The helical amorphous SiO₂ nanobelt samples were produced by thermal evaporation. Si monoxide powders (99.99% purity) placed in an alumina crucible on one side of an alumina boat were evaporated onto a series of cleaned Si (100) substrates located 9–15 cm away on the other side of the alumina boat. The alumina boat was inserted into an alumina tube with the alumina crucible located at the center of an electric heater. The alumina tube was evacuated to a pressure of 1×10^{-3} Pa, and 99.99% Ar was introduced as the carrier gas at 150 SCCM (SCCM denotes cubic centimeter per minute at STP) throughout the experiment, during which the alumina tube was heated to 1300 °C for 3 h. Finally, the alumina tube was cooled slowly to room temperature and the products were synthesized on the Si substrate.

Figures 1(a)–1(d) depict the general morphology of the products on Si (100) observed by scanning electron micros-

copy (SEM). Nanostructures several tens of micrometers long with helical pitches L (a whole repeat unit of helical belt) of about 3.2–3.8 μm are found on the substrate. The belt width W and thickness h are 400–800 and 40–80 nm, respectively. Figures 1(a) and 1(c) show helical nanobelts with $W=500$, 524 nm; $L=1.90$, 1.93 μm ; and $h=75$, 70 nm for a synthesis time of 180 min, whereas Figs. 1(b) and 1(d) display helical nanobelts with $W=1.25$, 1.39 μm ; $L=3.23$, 4.45 μm ; and $h=46$, 130 nm for a growth time of 160 min. It is important to point out that the SEM images of the samples produced with the shorter time [Figs. 1(b) and 1(d)] exhibit alternating dark and bright stripes on the nanobelt surfaces. The central axis parts [the white broken line in Fig. 1(b)] of the nanobelts are pale while the edge parts of nanobelts are bright. These stripes have a very orderly periodic structure and are distributed equally on two sides of the central axis. The spacing intervals l are equidistant but different nanobelts have different spacing intervals [$l=114$ nm in Fig. 1(b) and $l=174$ nm in Fig. 1(d)].

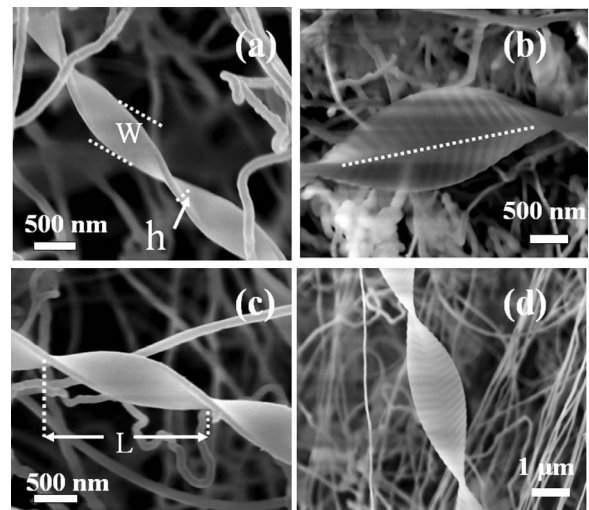


FIG. 1. SEM images of the helical amorphous twisted SiO₂ nanobelts. Images (a) and (c) are from the products with a longer synthesis time (180 min). Images (b) and (d) are from the products with a shorter growth time (160 min).

^{a)}Authors to whom correspondence should be addressed. Electronic addresses: hxlwu@nju.edu.cn and paul.chu@cityu.edu.hk.

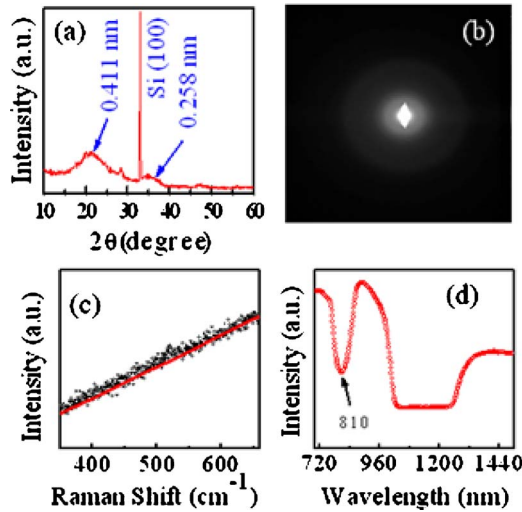


FIG. 2. (Color online) (a) XRD spectra, (b) SAED pattern, (c) Raman spectrum, and (d) FTIR spectrum of the amorphous Si oxide nanobelts.

The x-ray diffraction (XRD) pattern of the products is shown in Fig. 2(a). The pattern reveals two broad peaks arising from amorphous Si oxide, indicating that the product is composed of mainly amorphous Si oxide nanobelts. In order to accurately determine the helical nanobelt components, the selected-area electron diffraction (SAED) pattern is displayed in Fig. 2(b) and no light spots related to the crystalline component can be observed. Figures 2(c) and 2(d) present the Raman and Fourier transform infrared (FTIR) spectra. No Raman peak can be observed and it is indicative of the distinct amorphous Si oxide characteristics.²⁰ The FTIR peak at 810 cm^{-1} indicates that the Si and O ratio of the amorphous product is 1:2, and so the helical nanobelts comprise mainly of amorphous Si oxide.

Conventionally, amorphous Si oxide nanobelts will not roll themselves without an external load of surface stress. When we consider the existence of a thin crystalline Si oxide polar surface layer, the polar charges will cause the intrinsic stress.^{10,14} The spontaneous polarization dipole moment on the thin nanobelts with positively and negatively charged top and bottom surfaces increases the electrostatic, consequently forming the helical nanostructure to minimize or neutralize the overall dipole moment to form a stable shape, as illustrated in Fig. 3(a). We also conduct theoretical calculations according to the nanobelts structure model [Fig. 3(b)] to describe quantitatively the nanobelt surface changes. Previously, we have shown by high-resolution transmission electron microscopy that there exists a layer of thin crystalline SiO_2 on the side edge of the amorphous Si oxide nanobelt.¹⁴ The lattice spacing in the crystalline SiO_2 layer is about 0.51 nm, corresponding to the spacing of the (010) plane of the $\beta\text{-SiO}_2$ phase (cristobalite). The structure of the $\beta\text{-SiO}_2$ phase has many polar planes such as {100}, {101}, {201}, and {302}, which are vertical to the (010) plane. These polar planes have different charge types and densities. Because the polarization dipole moment on the nanobelts surface acts as the external stress to induce periodic deformation of the nanobelt surfaces, the periodic deformation will affect the charge distribution, thereby explaining the growth of the alternating dark and bright stripes observed experimentally. In addition, the deformation of the nanobelt edges is obviously larger than of the central axis part driving the charges to the

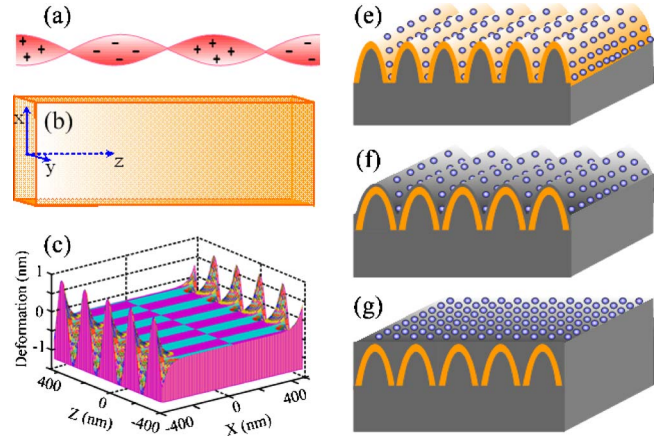


FIG. 3. (Color online) (a) A schematic model of a twisted nanobelt with positively and negatively charged top and bottom surfaces. (b) Calculation model of a nanobelt. (c) Simulated nanobelt surface deformation. Formation and disappearance of the bright and dark stripes on the helical twisted nanobelts: (d) The nanobelt surfaces with periodic deformation induced by the polar crystalline Si oxide layer and the stripes form. (e) The polar crystalline Si oxide layers are slowly covered by a newly grown amorphous Si oxide layer and the stripes become less apparent. (f) The nanobelt surfaces become smooth and the stripes vanish.

central part and leading to a pale central axis and a bright edge.

The elastic mechanical Poisson equation is introduced to explain theoretically why these stripes can appear on the nanobelt surface.²¹ Satisfying the rectangular region boundary conditions [as shown in Fig. 3(c)], the Poisson equation can be expressed as $\nabla^2\psi = -2G\phi$ and the Y direction shear stress $\tau_y = -\partial\psi/\partial x$. The stress function is

$$\psi = -G\phi \left[y^2 - \left(\frac{W}{2} \right)^2 + \frac{8W^2}{\pi^3} \sum_{1,3,5,\dots}^{\infty} \frac{\sin n\pi/2}{\cosh n\pi h/2W} \cosh \frac{n\pi x}{W} \cos \frac{n\pi y}{W} \cos \frac{\pi z}{l} \right],$$

where G and $\phi = \pi/2$ are the shear modulus and torsion angle. Clearly, the shear deformation can be affected significantly by the nanobelt periodic structure. Accordingly, the periodic deformation on the nanobelt surface can be simulated and the results are shown in Fig. 3(c). The surface charge density can be distributed periodically along the deformed surface. Figure 4 plots the stripe interval as a func-

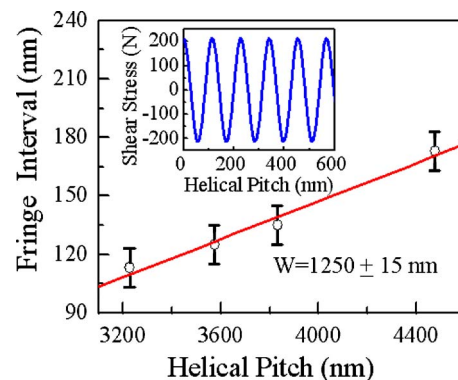


FIG. 4. (Color online) The fringe spacing intervals as a function of helical pitches for nanobelt widths in the range of 1250–1265 nm. The inset shows the shear stress as a function of helical pitches.

tion of the helical pitch (L) for a given nanobelt thickness and width. The stripe interval increases from 103 to 176 nm with increasing helical pitches. The intrinsic surface stress arising from the surface polarization dipole moment of the thin crystalline Si dioxide layer may be conceived as the external force that drives the periodic deformation. For the equivalent electrostatic energy, a larger helical pitch can dilute the charge density and decrease the per area shear stress, which is equivalent to increasing the strain period. To further determine clearly the shear stress behavior, the shear stress distribution as a function of helical pitches is shown in the inset of Fig. 4, which discloses a pronounced periodic stress distribution.

Figures 3(d)–3(f) schematically illustrates the formation and disappearance of the alternating dark and bright stripes. First, the electrostatic interaction of the positively and negatively charged top and bottom nanobelt surfaces [Fig. 3(d)] induces periodic deformation on the nanobelt surface, and then the charge density changes correspondingly from a uniform to a periodic distribution [Fig. 3(d)]. The higher electrical conductivity induced by a larger charge density in the valley is associated with the dark stripes, whereas the bright stripes correspond to the valley top with a smaller charge density. This schematic diagram can explain the stripe formation shown in Figs. 1(b) and 1(d). However, with increasing synthesis time, the newly grown amorphous Si oxide is only stable at the valley floor according to the lowest energy principle [Fig. 3(e)]. Hence, the charge density difference between the valley top and floor is reduced and the discrepancy between the dark and bright stripes becomes smaller. Finally, the polarized crystalline Si oxide layer is covered by newly formed amorphous Si oxide and the periodic deformation becomes smooth in order to decrease the electrostatic energy [Fig. 3(f)]. Thus, the uniform charge distribution eliminates the dark stripes resulting in bright uniform nanobelts [Figs. 1(a) and 1(c)].

In summary, we have observed foliaceous helical amorphous SiO₂ nanobelts from the products grown via a thermal evaporation technique. The elastic mechanical Poisson equation is employed to explain the observed periodic dark and

bright stripes on the nanobelt surfaces. Our results and mechanisms may explain the formation of other kinds of helical nanobelts.

This work was jointly supported by Grant Nos. 60876058, 60721063, BK2008020, and BK2006715 from the National and Jiangsu Natural Science Foundations. Partial support was also from National Basic Research Programs of China under Grant Nos. 2007CB936301 and 2006CB921803 as well as Hong Kong Research Grants Council (RGC) General Research Grant (GRF) Nos. CityU 112307 and CityU 112608.

¹S. Zhang, L. M. Peng, Q. Chen, G. H. Du, G. Dawson, and W. Z. Zhou, *Phys. Rev. Lett.* **91**, 256103 (2003).

²L. Z. Liu, G. S. Huang, L. L. Wang, T. H. Li, and X. L. Wu, *Appl. Phys. Lett.* **94**, 151903 (2009).

³S. B. Fagan, R. J. Baierle, and R. Mota, *Phys. Rev. B* **61**, 9994 (2000).

⁴X. T. An and J. J. Liu, *J. Appl. Phys.* **102**, 123706 (2007).

⁵L. Z. Liu and J. J. Liu, *J. Appl. Phys.* **102**, 033709 (2007).

⁶G. Germano, P. A. Michael, and J. Masters, *J. Chem. Phys.* **116**, 9422 (2002).

⁷F. Lu, W. P. Cai, Y. G. Zhang, Y. Li, and F. Q. Sun, *Appl. Phys. Lett.* **89**, 231928 (2006).

⁸B. Smith, Y. V. Zastavker, and G. B. Benedek, *Phys. Rev. Lett.* **87**, 278101 (2001).

⁹M. H. Zhao, Z. L. Wang, and S. X. Mao, *Nano Lett.* **4**, 587 (2004).

¹⁰H. F. Zhang, C. M. Wang, E. C. Buck, and L. S. Wang, *Nano Lett.* **3**, 577 (2003).

¹¹D. Q. Zhang, A. Alkhateeb, H. M. Han, H. Mahmood, and D. N. McIlroy, *Nano Lett.* **3**, 983 (2003).

¹²A. Katz and M. E. Davis, *Nature (London)* **403**, 286 (2000).

¹³H. W. Kim and S. H. Shim, *Appl. Surf. Sci.* **253**, 3664 (2007).

¹⁴Z. Y. Zhang, X. L. Wu, L. L. Xu, J. C. Shen, G. G. Siu, and P. K. Chu, *J. Chem. Phys.* **129**, 164702 (2008).

¹⁵X. Y. Kong and Z. L. Wang, *Nano Lett.* **3**, 1625 (2003).

¹⁶Z. W. Pan, Z. R. Dai, and Z. L. Wang, *Science* **291**, 1947 (2001).

¹⁷C. Ronning, P. X. Gao, Y. Ding, and Z. L. Wang, *Appl. Phys. Lett.* **84**, 783 (2004).

¹⁸X. Y. Kong and Z. L. Wang, *Appl. Phys. Lett.* **84**, 975 (2004).

¹⁹J. Liu, P. X. Gao, W. J. Mai, C. S. Lao, and Z. L. Wang, *Appl. Phys. Lett.* **89**, 063125 (2006).

²⁰N. Wang, Y. H. Tang, Y. F. Zhang, C. S. Lee, I. Bello, and S. T. Lee, *Chem. Phys. Lett.* **299**, 237 (1999).

²¹G. T. Yang, *Elastic Mechanics* (Higher Education, Beijing, 1998).